Article

Effect of a Compression Ratio Increase and High-Flow-Rate Injection on the Combustion Characteristics of an Ammonia Direct Injection Spark-Ignited Engine

Cheolwoong Park [1,*], Ilpum Jang [2], Jeongwoo Lee [2], Minki Kim [1], Chansoo Park [1], Yongrae Kim [1] and Young Choi [1]

[1] Korea Institute of Machinery and Materials, 156 Gajeongbuk-ro, Yuseong-gu, Daejeon 34103, Republic of Korea; kmk@kimm.re.kr (M.K.); cspark86@kimm.re.kr (C.P.); yrkim@kimm.re.kr (Y.K.); ychoi@kimm.re.kr (Y.C.)
[2] Department of Autonomous Vehicle System Engineering, Chungnam National University, 99 Daehak-ro, Yuseong-gu, Daejeon 34134, Republic of Korea; ipjang@cnu.ac.kr (I.J.); jwoo@cnu.ac.kr (J.L.)
* Correspondence: cwpark@kimm.re.kr; Tel.: +82-42-868-7928; Fax: +82-42-868-7305

Abstract: Despite efforts to use ammonia as a fuel, there remain problems with low combustion speeds and high unburned ammonia (NH_3) emissions. Therefore, methods to compensate for slow combustion speeds and stabilize combustion have been studied. This study aims to analyze how increasing the compression ratio affects engine performance to enhance thermal efficiency and reduce unburned emissions in a high-pressure ammonia direct injection spark-ignited engine. In addition, by applying a high-flow-rate (HFR) injector, an improvement in the combustion of ammonia fuel and exhaust gas emissions is observed through changes in the air–fuel mixture formation of high-pressure directly injected ammonia fuel. Compared with the existing compression ratio, the incomplete combustion loss due to unburned NH_3 increases significantly, and the thermal efficiency does not increase under an increased compression ratio. When HFR injectors are applied with an increase in the compression ratio, the net work increases by 4.7%, as incomplete combustion and energy losses of fuel are reduced by reducing the amount of unburned NH_3.

Keywords: ammonia; in-cylinder direct injection; compression ratio; thermal efficiency; high-flow-rate injector; energy loss

1. Introduction

Achieving carbon neutrality requires a radical energy transition from the current fossil-fuel-based energy system to one that actively utilizes renewable energy. Although hydrogen, as a candidate future energy source to replace fossil fuels, is considered a key material for realizing a carbon-neutral society, current hydrogen storage technology is limited by an insufficient energy per volume, making efficient storage and transportation difficult. Currently, high-pressure compression at 70 MPa or cryogenic liquefaction at 20 K is widely used to increase energy storage density. In addition to these physical methods, chemical methods using hydrogen carriers have been considered to maximize energy storage density [1]. Ammonia and various hydrocarbon-based fuels can be synthesized from hydrogen and applied to existing liquid-fuel-oriented infrastructure.

Green ammonia, synthesized using green hydrogen based on carbon-free energy sources, has no carbon emissions during production and consumption, and there has been significant technological progress for its direct use as a carbon-free combustion fuel or

feed material for solid oxide fuel cells [2]. In particular, ammonia ships have been actively researched in the shipping field, and both the direct use of ammonia and the indirect use of hydrogen through reformation have been being considered [3,4]. However, like hydrogen, the combustion characteristics of ammonia differ from those of common fuels. Ammonia has a slow flame speed, high auto-ignition temperature and ignition energy, and a narrow flammability limit at concentrations of 15–25% by volume in air. Therefore, the combustion conditions of ammonia-only combustion engines are unstable when under extremely small or large loads [5,6]. Therefore, it is preferable to use ammonia with auxiliary fuels, such as hydrogen or gasoline, in dual-fuel engines to increase reactivity rather than combustion alone [7,8]. In addition, large amounts of nitrogen oxide (NO_x) fuel can be generated by oxidizing nitrogen components during ammonia combustion [9]. Ammonia is known to corrode metals, such as copper, rubber, and plastic; therefore, it is necessary to review the lifespan and corrosion prevention of fuel system components [10]. In addition, ammonia is toxic to the human body; therefore, care must be taken when handling it.

Ammonia may initially appear unsuitable as engine fuel because of its high self-ignition temperature. However, its stoichiometric air–fuel ratio is 6.045, which is lower than that of other fuels. As a result, the calorific value of the fuel–air mixture is comparable to or higher than that of conventional fuels, such as gasoline and diesel. This means that even with current mass-produced engines, a reduced air intake can still generate a power output equivalent to or greater than that of traditional fuels. As the octane number is high (over 130), it is suitable for the development and operation of engines with an ignition source through a spark plug, such as a gasoline engine [11]. Previous studies have reported that it is possible to develop an engine using only pure ammonia fuel using an existing electric ignition engine or a diesel-engine-based high-compression-ratio engine. However, the development of successful engines has been limited by difficulties in configuring their intake and fuel supply systems [12,13]. In particular, for a stable supply of gaseous fuel to the intake manifold, the supply pressure can be maintained only by maintaining the temperature of the fuel container where liquid ammonia vaporizes. The Chinese company Guangzhou Automobile Group (GAC), a long-term partner of Toyota, unveiled an innovative internal combustion engine powered by ammonia during Tech Day, the annual technology event of the company, in summer 2024. The GAC prototype is a 2-L four-cylinder ammonia engine with an output of 161 HP that does not use forced induction and has 90% lower carbon emissions than a fossil fuel engine with the same capacity and output [14]. Wärtsilä in Finland announced in July 2021 that it had successfully tested a 70% ammonia co-fired engine at a typical ship propulsion load and planned to complete the development of a four-stroke ammonia full-fired medium-sized engine by 2023 [7].

Hegab et al. [15] reported research results on efficiency and exhaust gas characteristics according to the increase in ammonia replacement rate by using a small amount of diesel fuel as an ignition source in a diesel engine with a high compression ratio. Ambalakatte et al. [16] examined the effect of jet ignition under the condition of mixing minimal hydrogen to expand the operating range of an ammonia-fueled engine with poor ignition properties. Although much research [17–20] is still ongoing, engines that use only ammonia fuel have yet to be successfully developed.

Therefore, in a gasoline-based engine, the method of introducing sufficient air into the combustion chamber and then directly injecting a large amount of fuel is the most promising. However, in the case of fuel pumps and injectors, which are the most important components in the fuel supply system, parts must be replaced after confirming reactivity with ammonia, and low-viscosity ammonia fuel must be increased to high pressure. In previous research, areas were identified in which stable engine combustion was possible by high-pressure direct injection of ammonia fuel in an actual multi-cylinder ignition engine using an existing

liquefied petroleum gas (LPG) fuel supply system, and it was reported that expansion of the operating range was possible through the addition of hydrogen [5]. However, despite efforts to use ammonia as a fuel, because of problems with low combustion speeds and high unburned ammonia (NH_3) emissions, methods to compensate for slow combustion speeds and stabilize combustion have been studied [21,22].

A critical factor in developing ammonia engines is improving the combustion stability and efficiency and the ratio of brake work performed by an engine to the heating value of the fuel input by achieving optimal combustion as close to the top dead center (TDC) as possible. In this study, one approach involves increasing the compression ratio of the engine to enhance the thermal efficiency and burning speed by increasing the temperature and pressure of the unburned gas trapped in the cylinder. Considering that ammonia fuel has a high knocking resistance, knocking problems do not occur as in gasoline fuel; therefore, it is expected to improve fuel efficiency at high loads [11]. This approach not only improves fuel efficiency but also reduces unburned NH_3 emissions as much as possible. This study aims to examine the changes in combustion characteristics by increasing the compression ratio and changing the piston of an existing high-pressure ammonia direct injection spark-ignited engine. In addition, by applying a high-flow-rate (HFR) injector, an improvement in the combustion efficiency and exhaust gas characteristics is observed through changes in the air–fuel mixture formation of high-pressure directly injected ammonia fuel.

2. Materials and Methods

2.1. Experimental Apparatus

Table 1 lists the specifications of the LPG engine used to study the effect of varying compression ratios on the performance and efficiency of an ammonia combustion engine with a direct injection fuel supply system. The engine was a 2.5-L supercharged LPG model featuring a direct injection fuel injector that can handle fuel injection pressures up to 15 MPa. An injector with a modified O-ring and orifice material was installed to facilitate the delivery of ammonia fuel. Due to the corrosive nature of ammonia towards metals, such as copper, brass, zinc alloys, and aluminum brass, cracks or green corrosive compounds tend to form on these surfaces. As nitrile rubber (NBR) exhibits a low resistance to ammonia and deforms easily, it was essential to use rubber materials that are appropriate for handling ammonia.

Table 1. Specifications of the test engine.

Item	Specification
Displacement Volume [cc]	2497
Number of Cylinders [-]	4
Compression Ratio [-]	10.5
Bore × Stroke [mm]	88.5 × 101.5
Max. Torque [Nm]	300 @ 3800 rpm (w/LPG)
Max. Power [kW]	120 @ 3800 rpm (w/LPG)

Based on the original LPG engine, a piston with a compression ratio of 10.5 was employed, and several devices were added to support the high-pressure ammonia supply and control. To supply liquid ammonia, a low-pressure pump (EU YEON WESTEC) was used to prevent evaporation due to a decrease in supply pressure. A heat exchanger was used to prevent the temperature increase caused by the pressurized ammonia fuel and to control the temperature of the fuel. A schematic of the setup is shown in Figure 1. To further assess the effect of increased compression ratios, the piston was replaced, and the results were compared with those obtained with a compression ratio of 14.
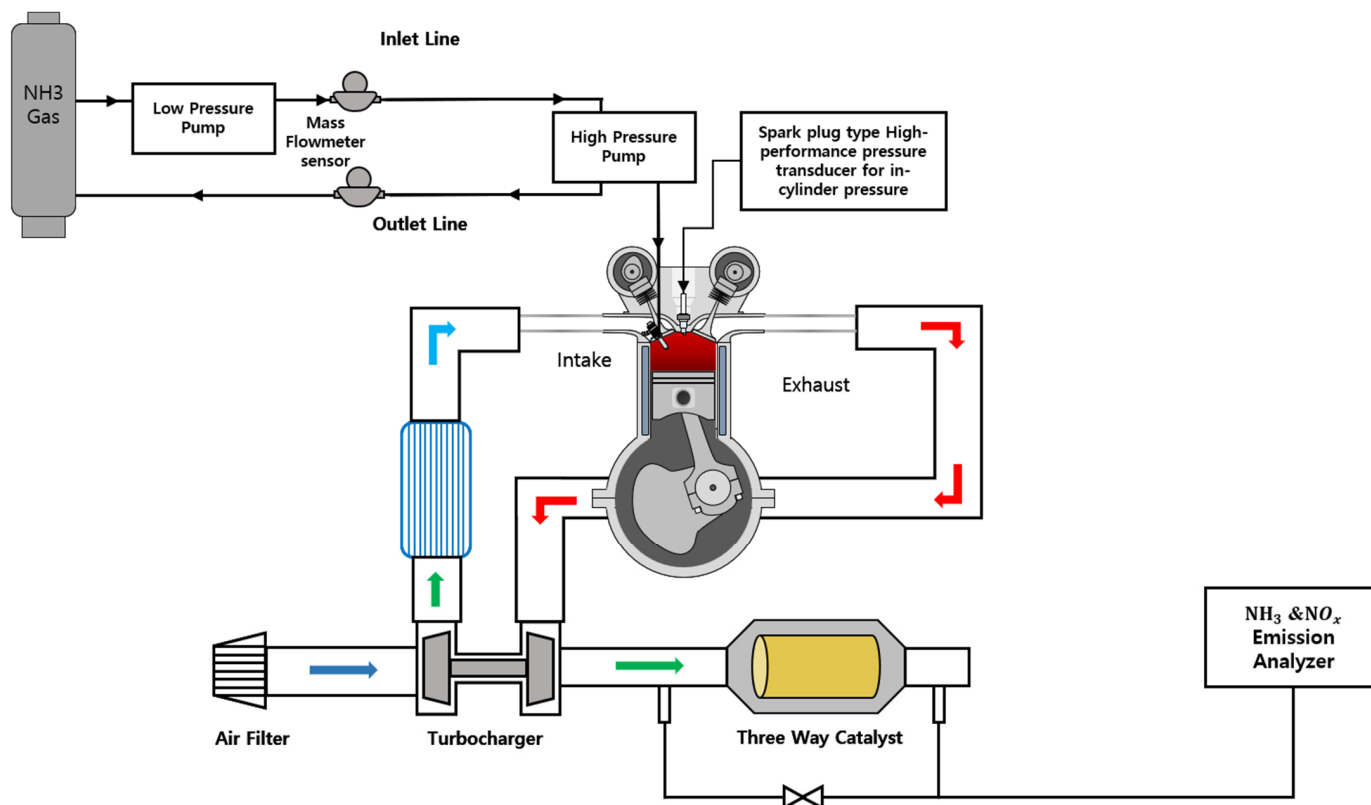
Figure 1. Schematic of the experimental setup.

Pure ammonia must be supplied from a low-pressure gas container in the liquid state to be adequately pressurized by a high-pressure fuel pump attached to the engine and delivered to the fuel injector. The general properties of ammonia are listed in Table 2. The HFR injector design, which doubled the number of holes compared with the original injector, increased the static flow rate by 67.6%. After increasing the fuel injection pressure to 15 MPa from the high-pressure pump, high-pressure liquid ammonia fuel was directly supplied to the combustion chamber through the injector, and the fuel supply pressure was constant regardless of the type of injector.

Table 2. Properties of ammonia fuel.

Item	Property
Chemical Formula [cc]	NH_3
Stoichiometric Air–Fuel Ratio [wt%]	6.0
Lower Heating Value [MJ/kg]	18.8
Research Octane Number [-]	130
Auto-ignition Temperature [K]	930
Min. Ignition Energy [mJ]	8
Laminar Flame Speed @ Stoichiometry [m/s]	0.1
Flammability Limits as Equivalence Ratio [-]	0.6–1.4

The fuel injection period, which was controlled by the engine control unit, regulated the supplied ammonia fuel, ensuring steady-state operation. A Coriolis-type mass flowmeter (CMFS010P, Micro-Motion) was used to measure the flow rate. Monitoring the engine control state allowed the acquisition of data on the fuel injection duration and ignition timing, which are crucial combustion control variables that affect engine performance. The engine speed and load were regulated using an alternating current (AC) dynamometer (INDY S33-2/0700-1BS-1). The combustion performance was gauged by measuring the

in-cylinder pressure data using a spark-plug-type pressure sensor (6113CF, Kistler) and a combustion analyzer (DEWE211, DEWETRON Co.), which calculated and displayed the heat release rate, in-cylinder temperature, and combustion stability using the acquired in-cylinder pressure in real time. Combustion stability, which is represented by the cyclic variability derived from the in-cylinder pressure data, is the coefficient of variation (COV) for the indicated mean effective pressure (IMEP) [23]. This value is calculated as the standard deviation of the IMEP divided by the mean IMEP and is usually expressed as a percentage. Generally, a COV$_{IMEP}$ value of 5% is the criterion for stable combustion. In addition, temperature and pressure sensors were installed to monitor key engine parts. The airflow rate was measured using a flowmeter with an ultrasonic transit-time differential technique (FSA 100, AVL). NO$_x$ emissions, mainly produced from the reaction of nitrogen and oxygen in air during combustion, and unburned NH$_3$, a by-product of incomplete combustion, were measured using an exhaust gas analyzer (SESAM FTIR, AVL). The uncertainty analyses are listed in Table 3 for each measured value, such as torque and pressure.

Table 3. Measurement range, accuracy, and uncertainty of measuring devices.

Parameter and Analyzer	Measurement Range	Accuracy	Uncertainty
Load cell for torque	0–700 Nm	±0.3% of full scale	±1.3 Nm (approx. 95% confidence level, k = 2)
Pulse pick-up unit for speed	0–7000 rpm	±1.5% of full scale	±61 rpm (approx. 95% confidence level, k = 2)
High-performance pressure transducer for intake air and exhaust gas pressures	0–1.0 MPa (absolute)	±0.25% of full scale	±0.002 MPa (approx. 95% confidence level, k = 2)
Mass flowmeter for ammonia flowrate	0–240 kg/h	±0.1% of measured value	±0.2 kg/h (approx. 95% confidence level, k = 2)
High-performance pressure transducer for in-cylinder pressure	0–15 MPa	±0.5% of full scale	±0.05 MPa (approx. 95% of confidence level, k = 2)
Thermocouple for exhaust gas temperature and coolant temperatures	−200–1250 °C	±0.75% of full scale	±2.2 deg C (approx. 95% of confidence level, k = 2)
NH$_3$ emissions analyzer (SESAM FTIR)	0–20,000 ppm	±1.0% of full scale	±231 ppm (approx. 95% confidence level, k = 2)
NO$_x$ and N$_2$O emissions analyzer (SESAM FTIR)	0–1000 ppm	±1.0% of full scale	±12 ppm (approx. 95% confidence level, k = 2)

The brake thermal efficiency is the ratio of the brake work performed by an engine to the lower heating value (LHV) of the fuel input and is calculated as follows:

$$\eta_{th} = \frac{W}{qLHV} \tag{1}$$

where W is the work, q is the fuel flow rate, and LHV is the lower heating value of the fuel input.

The first law of thermodynamics was applied, assuming a single area based on the combustion chamber of the engine.

$$dU = \delta Q - \delta W \tag{2}$$

where $U = C_v m T$, $\delta Q = \delta Q_{ch} - \delta Q_{ht}$, $\delta W = p dV$, U is the internal energy, C_v is the specific heat at a constant volume, m is the mass, T is the temperature, Q_{ch} is the heat release rate, Q_{ht} is the heat transfer, p is the pressure, and V is the volume.

$$\delta Q_{ch} = C_v dm T + C_v m dT + \delta Q_{ht} + p dV \tag{3}$$

Assuming that the gas movement in the combustion chamber is ideal, it is expressed as follows:

$$\frac{dp}{p} + \frac{dv}{V} = \frac{dm}{m} + \frac{dT}{T} \tag{4}$$

Substituting Equation (4) and $\gamma = \frac{C_p}{C_v} = 1 + \frac{R}{C_v}$ into Equation (3), where R is an ideal gas constant, yields:

$$\delta Q_{ch} = \frac{\gamma}{\gamma - 1} p dV + \frac{1}{\gamma - 1} V dp + \delta Q_{ht} \tag{5}$$

The heat release rate during combustion is expressed in Equation (5) as the sum of the two terms corresponding to the pressure and heat transfer amount.

The cooling loss is the heat lost from the burned gases through the cylinder wall to the coolant, which influences the thermodynamics of the engine cycle. It is calculated by subtracting the combustion loss from the total energy input of the fuel, as follows:

$$Q_{cooling} = qLHV(1 - Q_{combustion}) \tag{6}$$

where $Q_{cooling}$ is the cooling loss and $Q_{combustion}$ is the combustion loss.

2.2. Experimental Procedure

Previous research confirmed the feasibility of operating an engine solely with ammonia at various engine speeds and load conditions [6]. At an engine speed of 1000 rpm, stable operation with only ammonia was achievable, except under low-load conditions, where additional fuels such as hydrogen were unnecessary. In this study, the combustion characteristics of ammonia and changes in exhaust gas emissions with varying compression ratios were explored at an engine speed of 1000 rpm. Despite increasing the compression ratio, the anticipated efficiency improvements were not evident, prompting a further examination of the effects of using an HFR fuel injector.

The ignition timing was optimized for each operating condition to ensure operation at the minimum advance for the optimal torque ignition timing condition. The experimental conditions are listed in Table 4. Given the challenges in maintaining combustion stability, even with constant engine operating conditions and low temperatures for engine coolant and oil, experiments were conducted with the engine in a sufficiently warmed-up state ($90 \pm 2.5\ °C$).

Table 4. Engine operating parameters.

Item	Value
Intake valve opening [CAD, ATDC]	31
Intake valve closing [CAD, ABDC]	112
Exhaust valve opening [CAD, BBDC]	73
Exhaust valve closing [CAD, BTDC]	1
Spark ignition timing [CAD, BTDC]	25.5–42 (minimum spark advance for the best torque at each operating point)
Start of injection [CAD, BTDC]	360

3. Results and Discussion

3.1. Performance with an Increase in the Compression Ratio

First, the results of the improvement in the brake thermal efficiency (BTE) and combustion stability were examined as the compression ratio increased at an engine speed of 1000 rpm. As shown in Figure 2, as the compression ratio increased, the operating range was reduced to a condition where the maximum torque was 301.1 Nm, a decrease of approximately 7.8% compared with the existing compression ratio condition. The BTE increased up to the 200 Nm load condition and converged to approximately 37% at higher load conditions. The decrease in the BTE under load conditions of 200 Nm or less can be considered as the effect of pumping loss owing to a decrease in the intake pressure. Regardless of the compression ratio, at loads below 100 Nm, the variation in the COV_{IMEP} exceeded 5%, indicating inconsistent combustion behavior and contributing to a rapid decrease in BTE. However, combustion stability deteriorated as the compression ratio increased under all torque conditions. The BTE was at a similar level under all operating conditions, except for the lowest load operating condition, where there was a large difference in combustion stability, which showed a different trend from the expected improvement in the BTE as the compression ratio increased. In the case of the lowest load operating condition, the combustion stability deteriorated under the high-compression-ratio condition, and the BTE decreased slightly compared to the existing compression ratio condition.
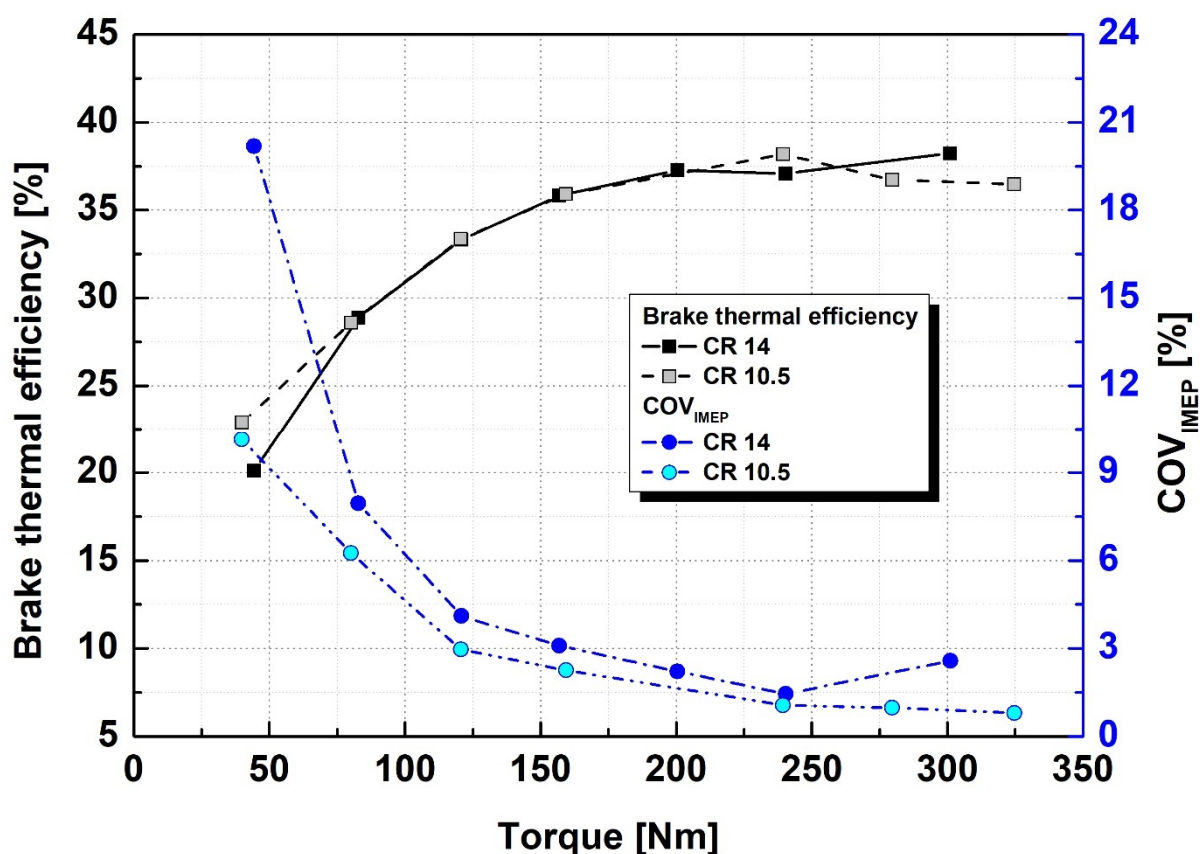

Figure 2. Brake thermal efficiency and combustion stability for an ammonia engine with compression ratio changes under various engine torques at 1000 rpm.

Accordingly, the results of the supplied fuel flow rate were examined, which directly affected the BTE under constant-torque conditions. Figure 3 shows the results of the ammonia fuel supply flow rate and exhaust gas temperature according to the load under the same operating conditions as shown in Figure 2. The flow rate of ammonia supplied to satisfy the load conditions was almost the same, regardless of the compression ratio.

However, under an increased compression ratio, the exhaust gas temperature decreased significantly, showing a difference of over 65 °C at a load condition of 80 Nm, and the temperature difference decreased as the load condition increased. This result shows that under high-compression-ratio conditions, the rate at which part of the input energy is lost owing to a decrease in the exhaust gas temperature decreases.
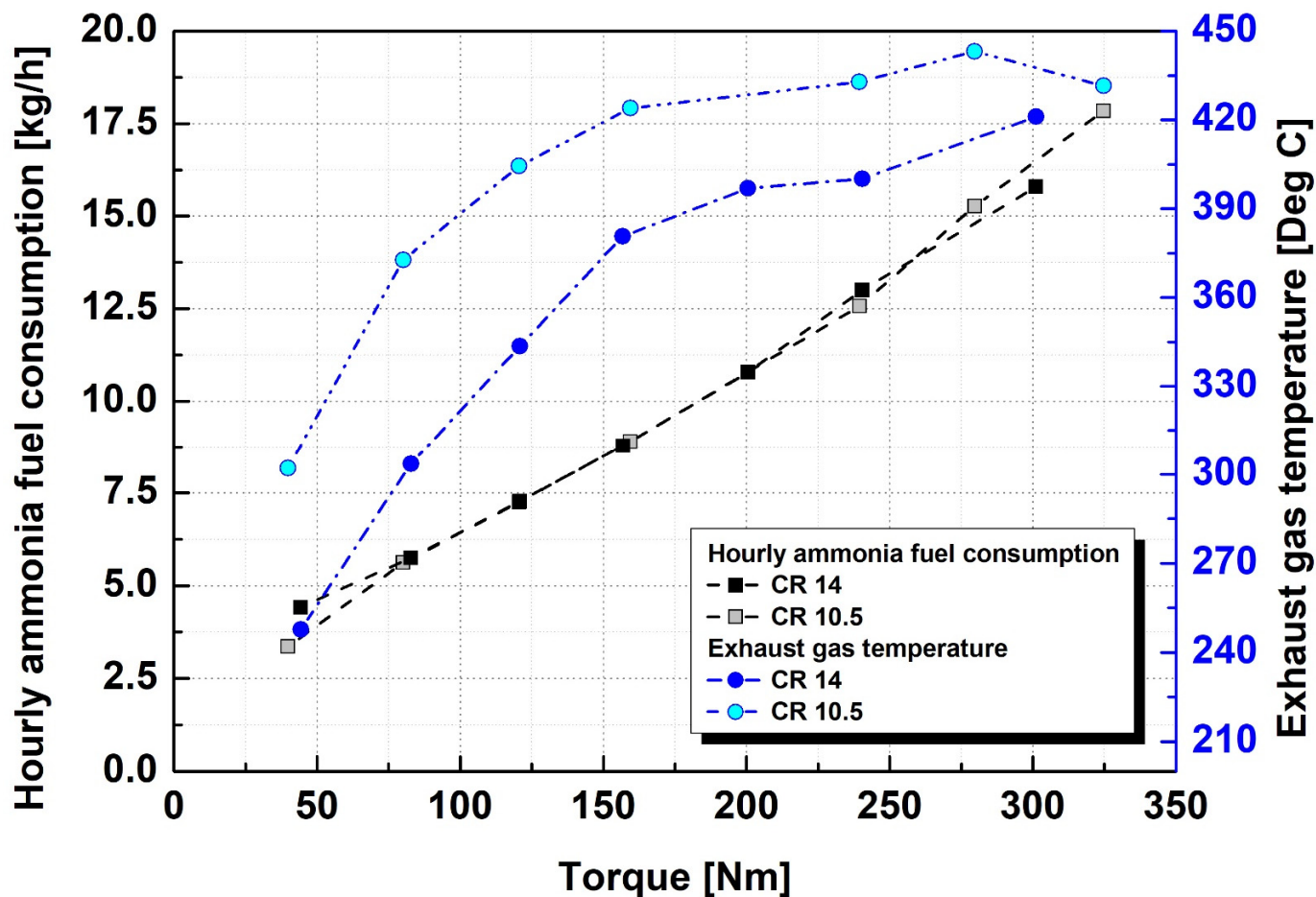

Figure 3. Ammonia fuel supply flow rate and exhaust gas temperature for an ammonia engine with compression ratio changes under various engine torques at 1000 rpm.

Considering that the energy input based on the supplied fuel was at the same level regardless of the change in the compression ratio, the fact that the overall BTE did not improve despite the decrease in the proportion of loss to exhaust energy indicates that energy was lost elsewhere. Figure 4 shows the emissions of NO_x and unburned NH_3 according to the changes in load. As the compression ratio increased, the overall NO_x emissions decreased slightly, and the emissions of unburned NH_3 increased significantly. Contrary to expectations, the combustion efficiency deteriorated under an increased compression ratio and increased unburned NH_3. The decrease in NO_x emissions can be attributed to a decrease in the combustion temperature due to an increase in the proportion of fuel that cannot participate in combustion under certain load conditions.

The calculated in-cylinder temperature and heat release rate for compression ratios of 10.5 and 14 were compared under a load of 120 Nm. As shown in Figure 5, the peak in-cylinder temperature calculated from the in-cylinder pressure was lower with an increased compression ratio. At the same ignition timing, when the compression ratio was increased, ignition occurred faster, but the peak heat release rate was lower than the trace of the heat release rate. The reason for this phenomenon is believed to be that the ammonia fuel injection timing of the high-pressure direct injection method occurred before top dead

center (BTDC) at a 360° crank angle degree (CAD), and the location of the piston used to increase the compression ratio was relatively close to the fire deck of the engine head. As the compression ratio increased from 10.5 to 14, the height of the central part of the upper surface of the piston increased and transformed into a flat shape, reducing the clearance volume. As the fuel injection timing was the same regardless of the compression ratio, a large amount of liquid fuel collided with and wetted the upper surface of the piston under high-compression-ratio conditions, where the piston was closer to the fire deck of the engine head. In the case of ammonia, which has a high latent heat of evaporation, a portion of the fuel injected directly at high pressure in liquid form cannot be fully evaporated until the point of ignition; however, the proportion of fuel droplets that failed to evaporate on the upper surface of the piston appeared to be higher under a high compression ratio. An increase in the thermal efficiency was expected when the compression ratio increased. However, unburned NH_3 increased owing to the wetting of ammonia fuel on the top surface of the piston and an increase in droplets rather than an increase in adiabatic compression and temperature owing to an increase in the compression ratio. Consequently, the combustion efficiency decreased, showing a similar level of thermal efficiency to the existing compression ratio conditions.
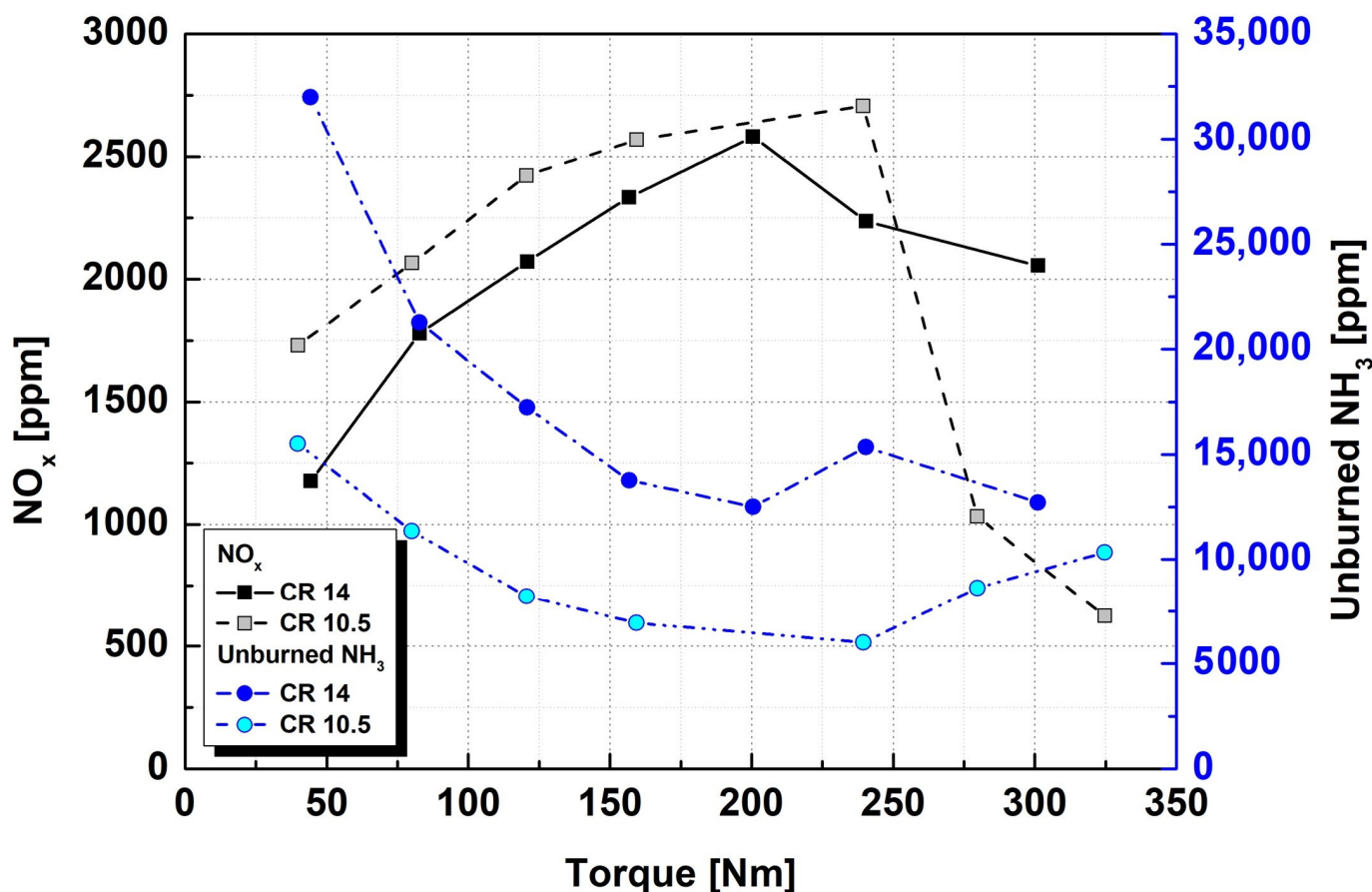

Figure 4. NO_x and unburned NH_3 emissions for an ammonia engine with compression ratio changes under various engine torques at 1000 rpm.
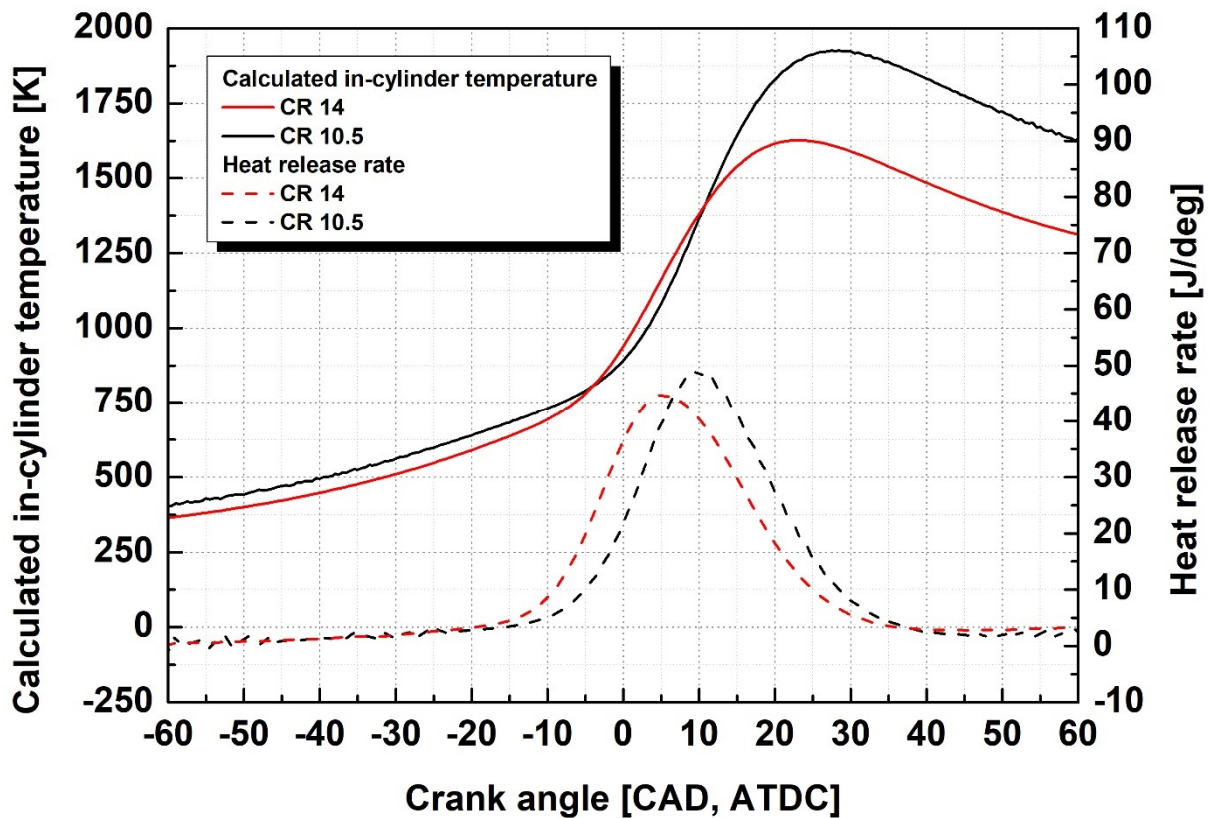
Figure 5. Calculated in-cylinder temperature and heat release rate traces for an ammonia engine with compression ratio changes at 120 Nm and 1000 rpm.

3.2. Effect of High-Flow-Rate Injectors

The expected improvement in thermal efficiency and expansion of the operating range were not achieved under an increased compression ratio. The cause of this phenomenon is believed to be that the liquid ammonia fuel that collided and wetted the upper surface of the piston did not evaporate completely until the point of ignition. HFR injectors were used to improve fuel supply characteristics. Figure 6 compares the calculated in-cylinder temperature and heat release rate when applying the HFR injector with those of the existing injector under increased compression ratio conditions. It can be seen from the heat release traces that all other control variables were under the same conditions, and the ignition timing was similar; however, the overall combustion period and heat release amount were reduced. Although the peak heat release rate was similar regardless of the injector type, the peak in-cylinder temperature was higher when the HFR injector was applied. This result shows that the combustion temperature increased because the amount of heat input was smaller, but the proportion of fuel participating in the combustion was higher.

When comparing the ammonia fuel supply flow rate and exhaust gas temperature when the HFR injectors were applied under the same operating conditions, as shown in Figure 7, the flow rate of the fuel supplied with the HFR injectors under similar load conditions was less than that under other conditions. This result indicates that the fuel consumption required to maintain certain operating conditions decreases owing to the increased thermal efficiency. The exhaust gas temperature was also similar to that in the case of a compression ratio of 14, indicating that the proportion of exhaust energy loss was not significantly different when the HFR injector was applied.
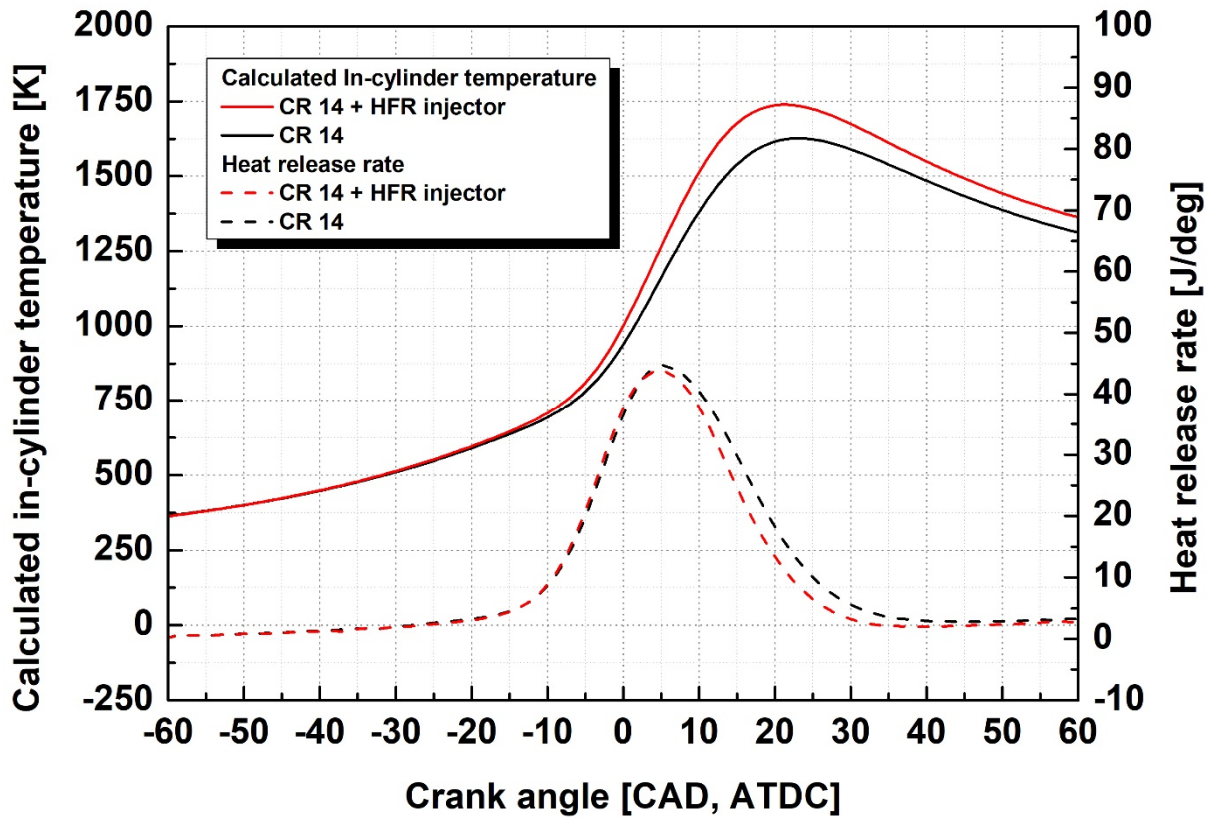
Figure 6. Calculated in-cylinder temperature and heat release rate traces for an ammonia engine with injector changes under a high compression ratio at 120 Nm and 1000 rpm.
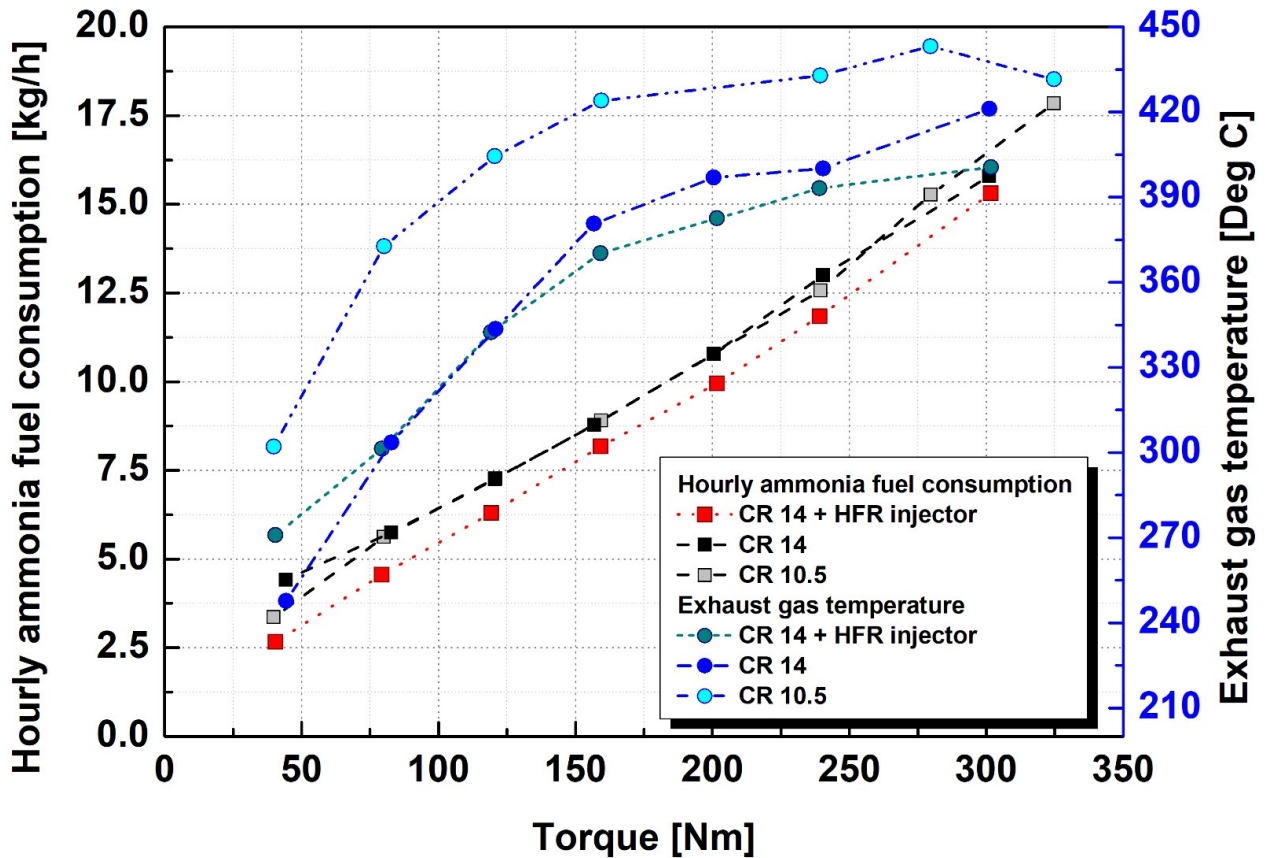

Figure 7. Ammonia fuel supply flow rate and exhaust gas temperature for an ammonia engine with compression ratio and injector changes under various engine torques at 1000 rpm.

As can be seen from the fuel injection period and the end of fuel injection timing results in Figure 8, the fuel injection period was reduced compared to other conditions depending on the application of the HFR injector. Based on the condition of 300 Nm, which is the longest fuel injection period, the reduction in the injection period of 5 ms was 39.9%, which was a sharp decrease compared to the 3% reduction corresponding to a fuel supply reduction of 0.48 kg/h. As the fuel injection period decreased, the end of the fuel injection timing advanced from BTDC 284 CAD to BTDC 314 CAD. As the piston descended from the TDC, the temperature and pressure in the combustion chamber decreased owing to the expansion. When the end of the fuel injection timing was advanced owing to the application of the HFR injector, the fuel injection ended under relatively high-temperature and high-pressure conditions; therefore, evaporation and mixing of the injected fuel with air were expected to occur more actively than under other conditions.
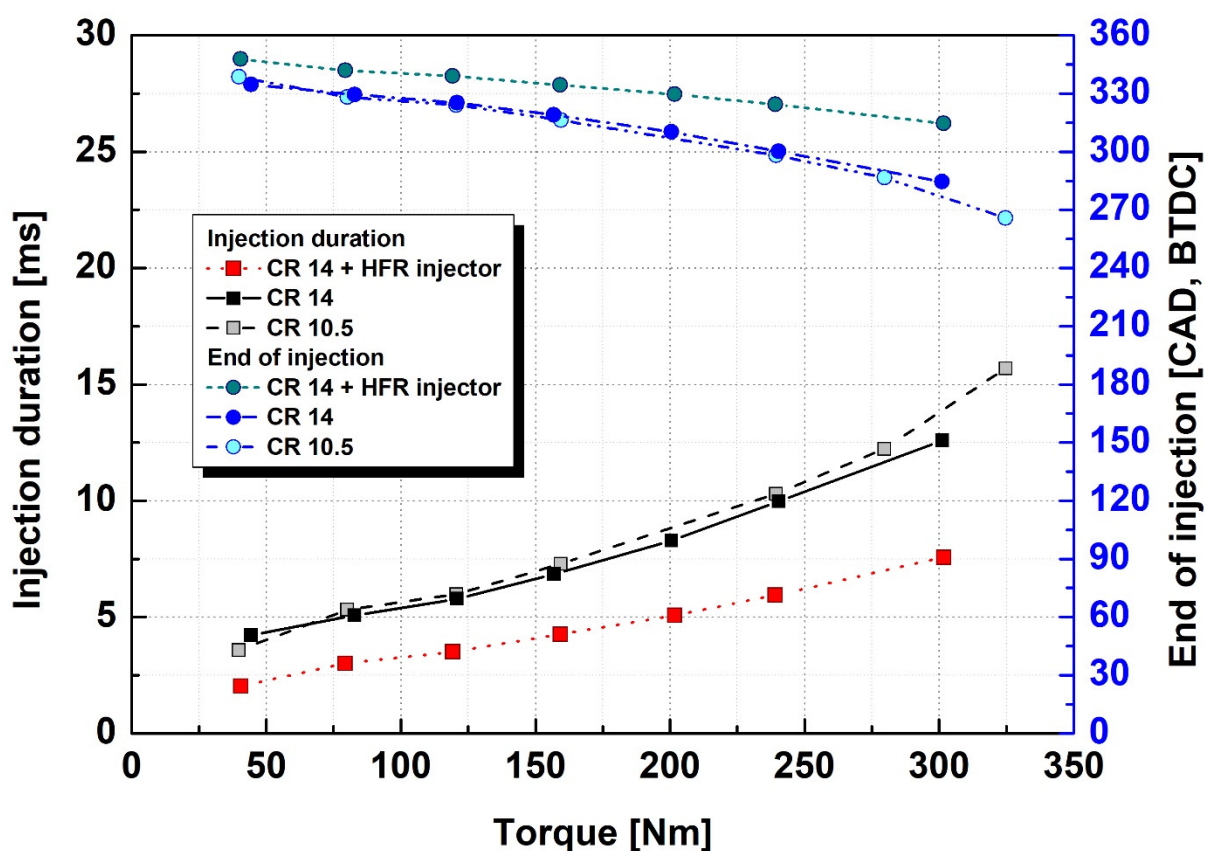

Figure 8. Ammonia fuel injection duration and end of fuel injection timing for an ammonia engine with compression ratio and injector changes under various engine torques at 1000 rpm.

Figure 9 shows the results of comparing the BTE and combustion stability when applying the HFR injector under the same operating conditions as shown in Figure 7. As the flow rate of ammonia supplied under constant load conditions decreased and the proportion of fuel participating in combustion increased, the BTE increased significantly, unlike other conditions showing the same level of BTE regardless of the compression ratio. In particular, the increase in the BTE was large under low-load conditions with low efficiency, showing an increase of 9% in BTE under the lowest load (40 Nm). The BTE increased even under high-load conditions, except for the 300 Nm operating condition, with an average increase of 3.3%. It appears that the significant increase in the BTE under low-load operating conditions was largely due to the improved combustion stability. When the HFR injectors were applied, relatively stable combustion with a COV$_{IMEP}$ value of 6% or less was confirmed under all load conditions.
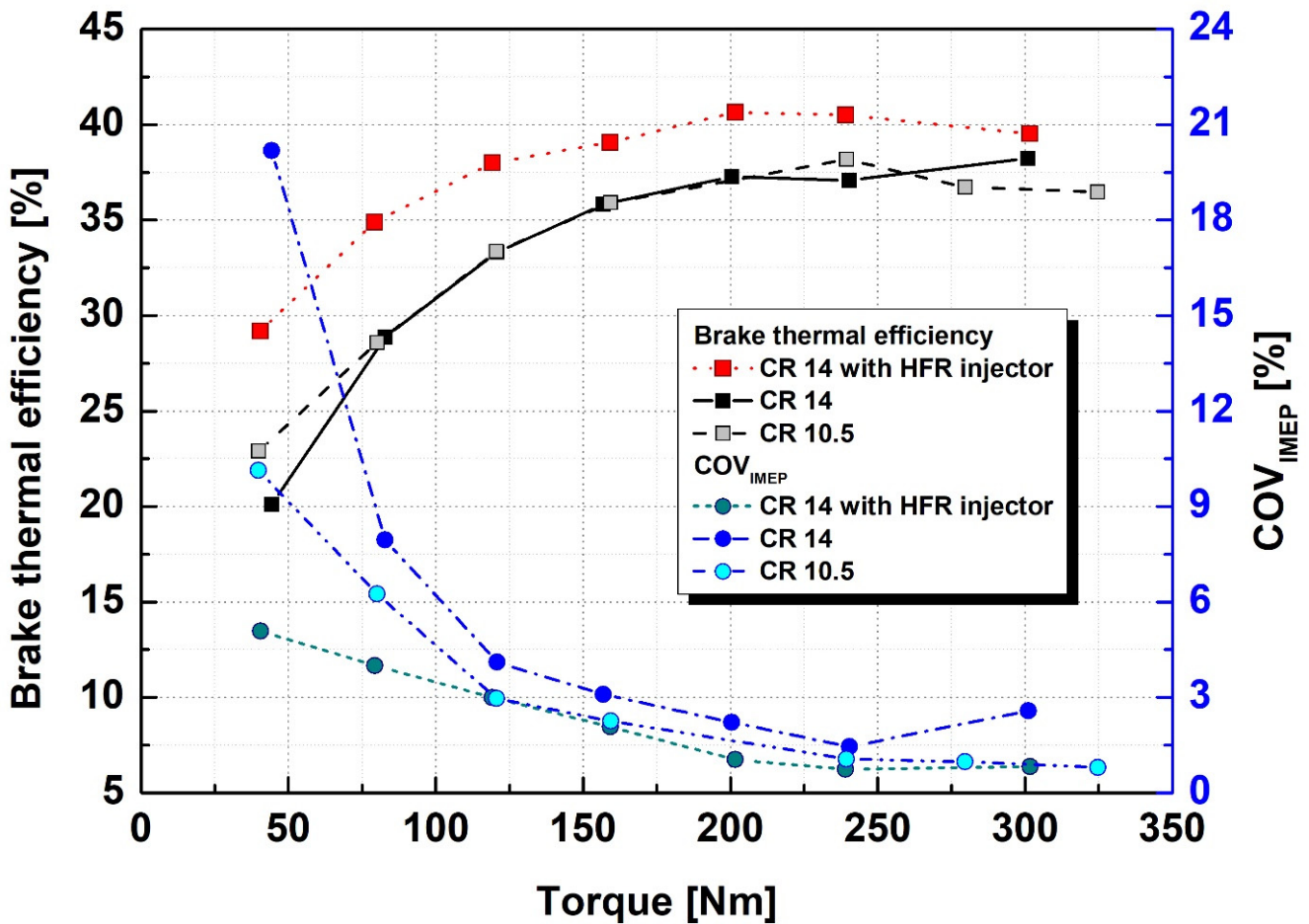
Figure 9. Brake thermal efficiency and combustion stability for an ammonia engine with compression ratio and injector changes under various engine torques at 1000 rpm.

The emission results for NO_x and unburned NH_3 according to the changes in each combustion control variable and load are shown in Figure 10. As expected from the calculated in-cylinder temperature results shown in Figure 6, the NO_x emissions increased owing to the increased combustion temperature in all operating ranges. The combustion efficiency improved with the application of HFR injectors, and unburned NH_3 decreased compared to the case of applying existing injectors but was still higher than that in the lower-compression-ratio condition. With the application of the HFR injector, the evaporation of the injected fuel and its mixing with air improved under high-compression-ratio conditions; however, the result appears to be unable to overcome the increase in fuel droplets that failed to evaporate on the upper surface of the piston, which increased compared to the low-compression-ratio condition. The highest value occurred under the lowest load condition of 40 Nm and decreased as the load increased; however, under high-load operation conditions of 200 Nm or more, the combustion efficiency decreased and tended to increase again. Combustion stability was secured under high-load operating conditions; however, this is believed to be due to the deterioration of combustion efficiency owing to the large absolute amount of fuel input. Regardless of the injector type, the decrease in combustion efficiency under high-load operating conditions of 240 Nm or more affected the combustion temperature, resulting in a tradeoff trend in which NOx emissions decreased.
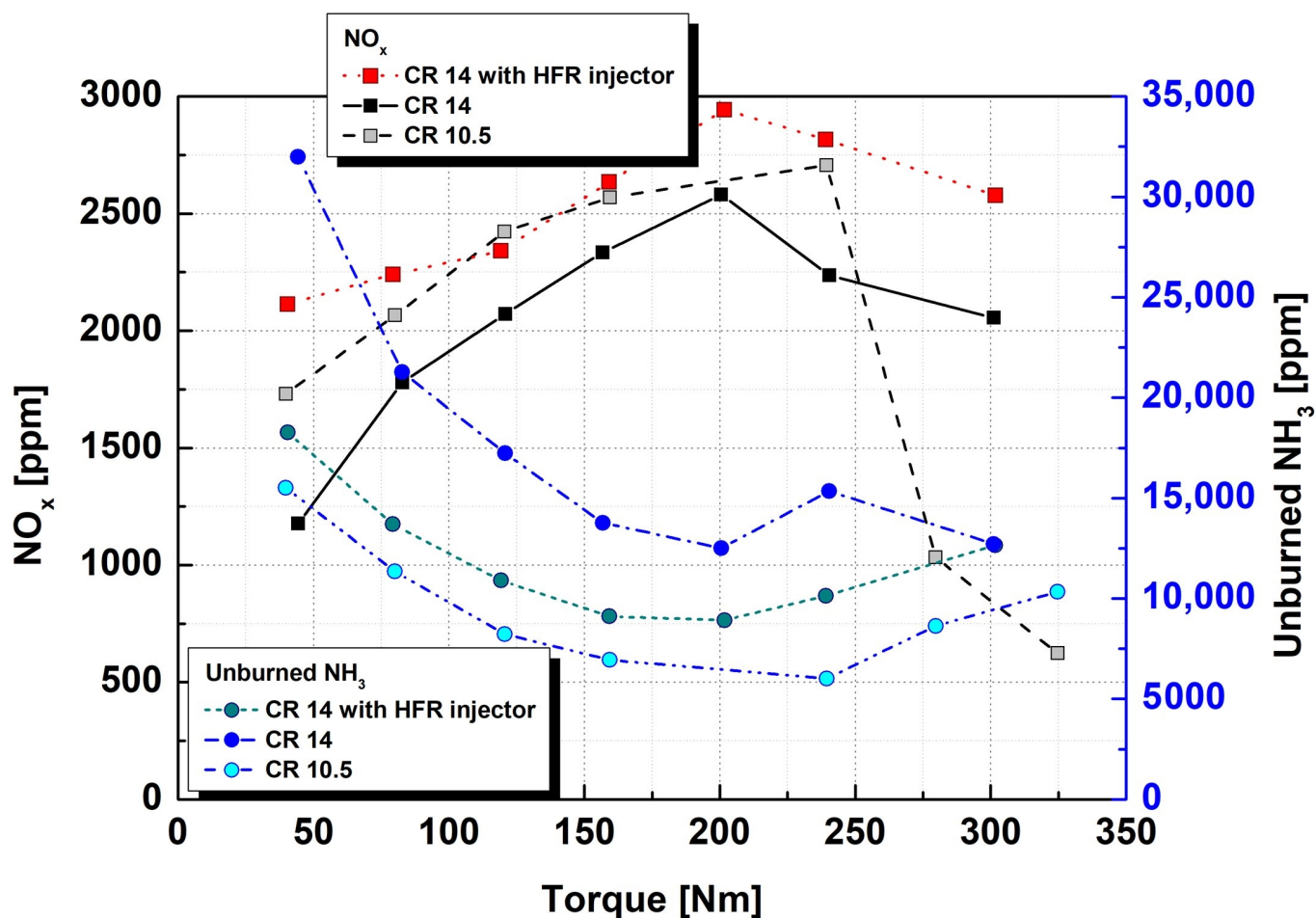
Figure 10. NO_x and unburned NH_3 emissions for an ammonia engine with compression ratio and injector changes under various engine torques at 1000 rpm.

To analyze how the effects of changes in control variables, such as compression ratio and HFR injector changes, were distributed under each condition, the cooling loss, incomplete combustion loss, and exhaust and friction were compared with the total input energy based on the amount of fuel supplied under the existing compression ratio condition in Figure 11 under the condition with an increased compression ratio and the condition using an HFR injector. The incomplete combustion loss is calculated from the measured unburned NH_3 mass, and the remaining unused energy comprises the exhaust and fraction losses. Compared to the existing compression ratio condition, the incomplete combustion loss due to unburned NH_3 increased significantly with an increased compression ratio. It is believed that the increase in friction caused by the geometric change of the pistons owing to the increase in the compression ratio affected the exhaust and friction losses. As the combustion temperature decreased, the cooling loss decreased significantly; however, the actual net work was similar. When HFR injectors were applied with an increase in the compression ratio, the combustion temperature increased, and the cooling loss slightly increased compared to the high-compression-ratio condition without HFR injectors. The proportion of net work for a selected engine operating condition increased by 4.7% as incomplete combustion and exhaust losses were reduced by reducing the unburned NH_3.
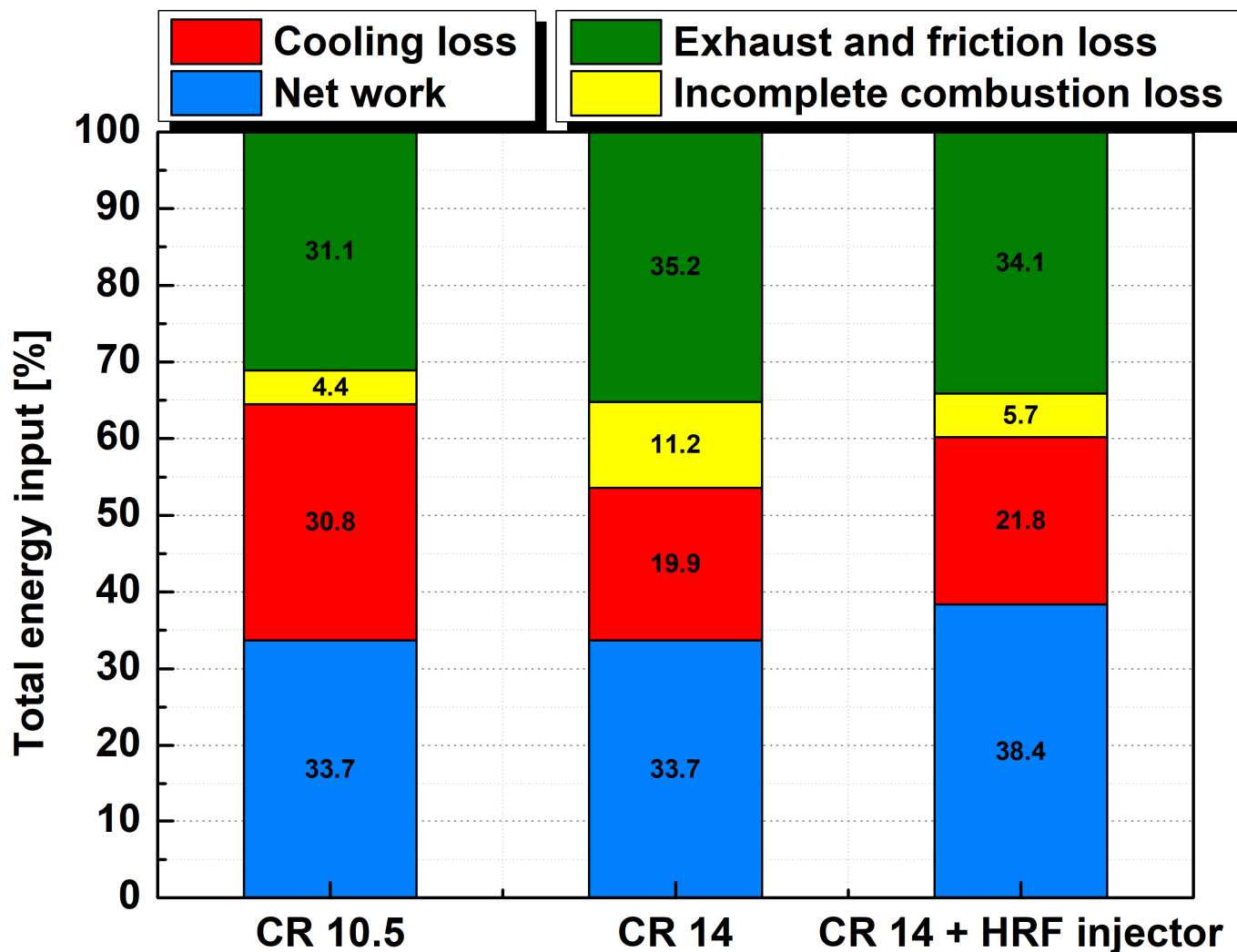
Figure 11. Energy breakdown for an ammonia engine with compression ratio and injector changes at 120 Nm and 1000 rpm.

4. Conclusions

In this study, the possibility of efficiency improvement was examined when a high-compression-ratio piston and an HFR injector were applied to a 2.5-L ammonia engine, and the combustion, exhaust, and efficiency results were experimentally compared and analyzed under each operating condition. The results are summarized as follows:

1. Even when the compression ratio of the ammonia high-pressure direct injection combustion engine increased, fuel evaporation and mixture formation worsened; thus, the exhaust gas temperature decreased, but the efficiency did not increase.
2. As the proportion of fuel wetted on the upper surface of the piston increased, the emission of unburned NH_3 increased by 30.3% and the combustion temperature decreased, thereby reducing NO_x emissions by 4.16%.
3. When the fuel injection period was reduced for the same amount of fuel using an HFR injector, the evaporation characteristics and mixture formation of the fuel were improved, and the fuel consumption decreased by 10.7%.
4. Applying HFR injectors reduced the emission of unburned NH_3 and increased the combustion temperature, thereby increasing the emission of NO_x.

5. When an HFR injector was applied, the incomplete combustion and exhaust losses were reduced, increasing the thermal efficiency by 4.7%. Finally, the thermal efficiency is improved with an HFR injector under high-compression-ratio conditions.

Author Contributions: Methodology, Y.K.; Validation, Y.C.; Formal analysis, J.L.; Investigation, C.P. (Chansoo Park); Resources, M.K.; Data curation, I.J.; Writing—original draft, C.P. (Cheolwoong Park); Supervision, C.P. (Cheolwoong Park); Project administration, Y.C. All authors have read and agreed to the published version of the manuscript.

Institutional Review Board Statement: Not applicable.

Informed Consent Statement: Not applicable.

Data Availability Statement: The data is confidential.

Conflicts of Interest: The authors declare no conflict of interest.

Abbreviations

The following abbreviations are used in this manuscript:

ABDC	After bottom dead center
ATDC	After top dead center
BTDC	Before top dead center
BBDC	Before bottom dead center
BTE	Brake thermal efficiency
CAD	Crank angle degree
COV_{IMEP}	Coefficient of variation for indicated mean effective pressure
HFR	High flow rate
LPG	Liquid petroleum gas
TDC	Top dead center

References

1. Scarpati, G.; Frasci, E.; Di Ilio, G.; Jannelli, E. A comprehensive review on metal hydrides-based hydrogen storage systems for mobile applications. *J. Energy Storage* **2024**, *102*, 113934. [CrossRef]
2. Lee, H.; Youngmin Woo, M.J.L. The needs for R&D of ammonia combustion technology for carbon neutrality—Part I Background and Economic Feasibility of Expanding the Supply of Fuel. *Korean Soc. Combust.* **2021**, *26*, 59–83.
3. Gallucci, M. The ammonia solution: Ammonia engines and fuel cells in cargo ships could slash their carbon emissions. *IEEE Spectr.* **2021**, *58*, 44–50. [CrossRef]
4. Kim, K.; Park, K.; Roh, G.; Choung, C.; Kwag, K.; Kim, W. Proposal of zero-emission tug in South Korea using fuel cell/energy storage system: Economic and environmental long-term impacts. *J. Mar. Sci. Eng.* **2023**, *11*, 540. [CrossRef]
5. Park, C.; Jang, Y.; Kim, S.; Kim, Y.; Choi, Y. Influence of hydrogen on the performance and emissions characteristics of a spark ignition ammonia direct injection engine. *Gases* **2023**, *3*, 144–157. [CrossRef]
6. Park, C.; Jang, Y.; Min, C.; Kim, Y.; Choi, Y.; Kim, M. Experimental investigation of operating conditions on performance and emissions of spark ignition ammonia direct injection engine. *Appl. Therm. Eng.* **2024**, *241*, 122382. [CrossRef]
7. Xu, L.; Xu, S.; Bai, X.-S.; Repo, J.A.; Hautala, S.; Hyvönen, J. Performance and emission characteristics of an ammonia/diesel dual-fuel marine engine. *Renew. Sustain. Energy Rev.* **2023**, *185*, 113631. [CrossRef]
8. Kurien, C.; Mittal, M. Review on the production and utilization of green ammonia as an alternate fuel in dual-fuel compression ignition engines. *Energy Convers. Manag.* **2022**, *251*, 114990. [CrossRef]
9. Kobayashi, H.; Hayakawa, A.; Somarathne, K.D.K.A.; Okafor, E.C. Science and technology of ammonia combustion. *Proc. Combust. Inst.* **2019**, *37*, 109–133. [CrossRef]

10. Jang, J.; Woo, Y.; Yoon, H.C.; Kim, J.-N.; Lee, Y.; Kim, J. Combustion characteristics of ammonia-gasoline dual-fuel system in a one liter engine. *J. Korean Inst. Gas.* **2015**, *19*, 1–7. [CrossRef]

11. Dimitriou, P.; Javaid, R. A review of ammonia as a compression ignition engine fuel. *Int. J. Hydrogen Energy* **2020**, *45*, 7098–7118. [CrossRef]

12. Pearsall, T.J.; Garabedian, C.G. Combustion of anhydrous ammonia in diesel engines. *SAE Trans.* **1968**, *76*, 3213–3221.

13. Starkman, E.S.; James, G.E.; Newhall, H.K. Ammonia as a diesel engine fuel: Theory and application. *SAE Trans.* **1968**, *76*, 3193–3212.

14. Miyagawa, H.; Suzuoki, T.; Nakatani, N.; Homma, T.; Takeuchi, Y. Reduction of cold-start emissions from an ammonia mono-fueled spark ignition engine. *Int. J. Hydrogen Energy* **2024**, *91*, 924–932. [CrossRef]

15. Hegab, A.; Bowling, W.; Cairns, A.; Harrington, A.; Hall, J.; Bassett, M. *Development of an Ultra-Low Carbon Flex Dual-Fuel Ammonia Engine for Heavy-Duty Applications*; SAE International: Warrendale, PA, USA, 2024. [CrossRef]

16. Ambalakatte, A.; Cairns, A.; Geng, S.; Varaei, A.; Hegab, A.; Harrington, A.; Hall, J.; Bassett, M. *Experimental Comparison of Spark and Jet Ignition Engine Operation with Ammonia/Hydrogen Co-Fuelling*; SAE International: Warrendale, PA, USA, 2024. [CrossRef]

17. Uddeen, K.; Almatrafi, F.; Shi, H.; Tang, Q.; Parnell, J.; Peckham, M.; Turner, J. Investigation into Various Strategies to Achieve Stable Ammonia Combustion in a Spark-Ignition Engine. *SAE Int. J. Adv. Curr. Pract. Mobil.* **2023**, *6*, 2102–2113. [CrossRef]

18. Uddeen, K.; Tang, Q.; Shi, H.; Magnotti, G.; Turner, J. *Multiple Spark Ignition Approach to Burn Ammonia in a Spark-Ignition Engine: An Optical Study*; SAE International: Warrendale, PA, USA, 2023. [CrossRef]

19. Mounaïm-Rousselle, C.; Bréquigny, P.; Dumand, C.; Houillé, S. Operating Limits for Ammonia Fuel Spark-Ignition Engine. *Energies* **2021**, *14*, 4141. [CrossRef]

20. Lhuillier, C.; Brequigny, P.; Contino, F.; Mounaïm-Rousselle, C. Experimental investigation on ammonia combustion behavior in a spark-ignition engine by means of laminar and turbulent expanding flames. *Proc. Combust. Inst.* **2021**, *38*, 5859–5868. [CrossRef]

21. Mørch, C.S.; Bjerre, A.; Gøttrup, M.P.; Sorenson, S.C.; Schramm, J. Ammonia/hydrogen mixtures in an SI-engine: Engine performance and analysis of a proposed fuel system. *Fuel* **2011**, *90*, 854–864. [CrossRef]

22. Frigo, S.; Gentili, R. Analysis of the behaviour of a 4-stroke Si engine fuelled with ammonia and hydrogen. *Int. J. Hydrogen Energy* **2013**, *38*, 1607–1615. [CrossRef]

23. Heywood, J.B. *Internal Combustion Engine Fundamentals*; McGraw-Hill: New York, NY, USA, 1988.